AIAA 95-0304

A Numerical Method for Solving Cascade Inverse Problems Using Navier - Stokes Equations

Z. Wang
Institute of Engineering Thermophysics
Beijing, People's Republic of China

and

G. S. Dulikravich
The Pennsylvania State University
University Park, PA

33rd Aerospace Sciences Meeting and Exhibit
January 9-12, 1995 / Reno, NV

A NUMERICAL METHOD FOR SOLVING CASCADE INVERSE PROBLEMS USING NAVIER-STOKES EQUATIONS

Zhengming Wang*
Institute of Engineering Thermophysics
Chinese Academy of Sciences
Beijing 100080
People's Republic of China

George S. Dulikravich**
Department of Aerospace Engineering
The Pennsylvania State University
University Park, PA 16802

Abstract

A new numerical method for solving inverse aerodynamic shape design problem of airfoils in a linear periodic cascade using a fully-viscous compressible flow model has been developed. The general inverse problem refers to the problem in which the pressure distributions on suction and pressure surfaces of the airfoil are given, but the corresponding airfoil shape is unknown. The calculations are performed directly in the physical plane by Navier-Stokes equations employing nonorthogonal curvilinear H-type grid and nonorthogonal velocity components. In this article, the MacCormack's explicit time-marching algorithm with Baldwin-Lomax turbulence model are adopted as the basic flow solver. In order to satisfy the specified surface pressure distribution, the blade surface points move regularly with integration time steps until zero surface normal velocity is reached. Comparison of numerical and experimental results indicates that the method is very effective.

Nomenclature

c_p	specific heat at constant pressure
C_p	pressure coefficient=$2(p_{o\,-oo} - p)/(\rho_{-oo}(w)^2_{-oo})$
$\mathbf{e}_i$	base vector of x^i coordinate system
$\mathbf{e}^i$	reciprocial base vector of x^i coordinate system
g	Jacobian of the matrix g_{ij}
g_{ij}	covariant metric tensor of x^i coordinate system
g^{ij}	contravariant metric tensor of x^i coord. system
h	enthalpy per unit mass
n	number of iterations
p	thermodynamic pressure
P	point in the flow field or on the airfoil
R	specific gas constant
r,ϕ,z	cylindrical coordinates
T	absolute temperature
t	time, or spacing between airfoils in a cascade
$\mathbf{w}$	fluid velocity vector
w_i	covariant component of fluid velocity vector
w^i	contravariant physical component of fluid velocity vector
x^i	nonorthogonal curvilinear coordinates
Γ^k_{ij}	Christoffel symbol of the second kind
$\Delta\phi$	$\Delta\phi = t / r - (\phi_p - \phi_s)$
k	coefficient of thermal conductivity of the fluid
μ	coefficient of shear (molecular) viscosity
μ_t	coefficient of turbulent viscosity
Π_{ij}	elements of the viscous stress tensor
ρ	fluid density
σ	total pressure recovery coefficient $\sigma = p_o / p_{o\,-oo}$

Subscripts

o	stagnation
-oo	inlet boundary
+oo	exit boundary
p	pressure surface
s	suction surface

---

* Associate Research Professor.

** Associate Professor. Associate Fellow AIAA.

Introduction

The aerodynamic design of high-performance turbomachinery blades is presently performed by combining a quasi three-dimensional inverse design with a fully three-dimensional analysis process[1,2]. The numerical simulations of the two-dimensional and three-dimensional inverse problems will play very important role in the design system (Figure 1) leading the optimization of turbomachinery blade shapes.

A variety of schemes for solving inverse and mixed-type shape design problems have been developed[3-8] in order to improve the design of turbomachinery airfoil cascades[9-14]. In practice, better results have been obtained by combining direct problem (analysis) schemes with the inverse (design) problem schemes[14-16]. However, most of these methods are based on the inviscid flow models. To adequately represent the physics of the flow, it is necessary to consider the fluid viscosity in the solution of the inverse problem as well as in the direct problem of cascade flows. The two usual methods for considering the influence of fluid viscosity are the interacting viscous/inviscid approach[17,18,16] and the method of directly solving some form of the Navier-Stokes equations. The former approach has the advantage of being simpler and faster, although it is less robust and it cannot adequately resolve flow separation region, shock/boundary layer interaction, wake flow, etc.

In this paper, the numerical method for directly solving viscous inverse problem using Navier-Stokes equations is attempted. Based on the equations derived in non-orthogonal curvilinear boundary-conforming coordinates and corresponding non-orthogonal velocity vector components, the explicit time-marching algorithm is adopted and the boundary conditions on the surfaces of the airfoil cascade are treated in a special manner. In the iterative process, the airfoil surfaces are movable like the elastic film shapes that change when subjected to the desired surface pressure distribution.

Governing Equations

Based on nonorthogonal curvilinear coordinates and corresponding nonorthogonal velocity components[19], the following governing equations written in conservative form are employed[20,21] using tensor notation.

Mass conservation:

$$\frac{\partial(\sqrt{g}\rho)}{\partial t} + \frac{\partial}{\partial x^i}\left(\frac{\sqrt{g}}{\sqrt{g_{ii}}}\rho w^i\right) = 0 \tag{1}$$

Momentum conservation in circumferential direction:

$$\frac{\partial}{\partial t}\left(\frac{\sqrt{g}}{\sqrt{g_{jj}}}\rho w^j \vec{e}_j\cdot\vec{e}_1(P)\right)$$

$$+\frac{\partial}{\partial x^i}\left(\frac{\sqrt{g}}{\sqrt{g_{ii}}\sqrt{g_{jj}}}\rho w^i w^j \vec{e}_j\cdot\vec{e}_1(P)\right)$$

$$+\frac{\partial}{\partial x^i}\left(\sqrt{g}\, p\, \vec{e}^i\cdot\vec{e}_1(P)\right)$$

$$+\frac{\partial}{\partial x^i}\left(-\Pi_{j\alpha} g^{\alpha i}\sqrt{g}\ \vec{e}^j\cdot\vec{e}_1(P)\right) = 0 \tag{2}$$

Momentum conservation in locally streamwise direction:

$$\frac{\partial}{\partial t}\left(\frac{\sqrt{g}}{\sqrt{g_{jj}}}\rho w^j \vec{e}_j\cdot\vec{e}_2(P)\right)$$

$$+\frac{\partial}{\partial x^i}\left(\frac{\sqrt{g}}{\sqrt{g_{ii}}\sqrt{g_{jj}}}\rho w^i w^j \vec{e}_j\cdot\vec{e}_2(P)\right)$$

$$+\frac{\partial}{\partial x^i}\left(\sqrt{g}\, p\, \vec{e}^i\cdot\vec{e}_2(P)\right)$$

$$+\frac{\partial}{\partial x^i}\left(-\Pi_{j\alpha} g^{\alpha i}\sqrt{g}\ \vec{e}^j\cdot\vec{e}_2(P)\right) = 0 \tag{3}$$

Energy conservation:

$$\frac{\partial}{\partial t}\left(\sqrt{g}(\rho h_o - p)\right) + \frac{\partial}{\partial x^i}\left(\frac{\sqrt{g}}{\sqrt{g_{ii}}}\rho w^i h_o\right)$$

$$+\frac{\partial}{\partial x^i}\left(-\sqrt{g}\ g^{ij}\lambda\frac{\partial T}{\partial x^j}\right)$$

$$+\frac{\partial}{\partial x^i}\left(-\frac{\sqrt{g}}{\sqrt{g_{kk}}} g^{ij}\Pi_{jk} w^k\right) = 0 \tag{4}$$

Equation of state for a thermally perfect gas:

$$p = \rho R T \tag{5}$$

Stagnation enthalpy per unit mass:

$$h_o = c_p T + (w)^2/2 \tag{6}$$

where

$$(w)^2 = g_{\alpha\beta}\frac{w^\alpha}{\sqrt{g_{\alpha\alpha}}}\frac{w^\beta}{\sqrt{g_{\beta\beta}}} \tag{7}$$

Here, x^1 is along circumferential direction and x^2 is along the local streamwise direction on the airfoil surface. Elements of the viscous stress tensor are

$$\Pi_{ij} = \mu \left(\frac{\partial w_j}{\partial x^i} + \frac{\partial w_i}{\partial x^j} - 2 w_k \Gamma^k_{ij} - \frac{2}{3} g_{ij} \nabla \cdot \mathbf{w} \right) \quad (8)$$

where Christoffel symbols of the second kind are

$$\Gamma^k_{ij} = \frac{1}{2} g^{hk} \left(\frac{\partial g_{ih}}{\partial x^j} + \frac{\partial g_{jh}}{\partial x^i} - \frac{\partial g_{ij}}{\partial x^h} \right) \quad (9)$$

Turbulence was modeled using Baldwin-Lomax turbulence model[22]. This paper describes one of the first-known attempts to develop a useful-shape inverse design code that utilizes Navier-Stokes equations and accounts for compressibility, flow separation and turbulence effects.

Numerical Method

The MacCormack's explicit predictor-corrector time marching scheme[23] was used in the numerical solution of the compressible Navier-Stokes equations. In the calculation of inverse problem, because the airfoil profile is unknown beforehand, an initial profile shape must be provided. In principle, the initial shape may be selected within a wider range of realistic configurations. The computational process for the inverse problem is similar to the more common direct problem, but the manner of treating boundary conditions on airfoil surfaces is different. In the direct problem, the no-slip condition is imposed at the blade surfaces, that is $w^2 = w^1 = 0$.

In the inverse problem, the surface pressure distribution, which is obtained from the specified pressure coefficient distribution, is enforced iteratively together with $w^2 = 0$. This will result in $w^1 \neq 0$ on the pressure and suction surfaces. Hence, the airfoil surfaces could be moved in the x^1 direction by the amount $w^1 \Delta t$ with each iteration time steps until the convergence is reached, that is, until $w^1 = 0$ is satisfied on the final surface configuration. This concept requires only minor modification in a boundary conditions subroutine of any standard flow analysis code since it is essentially a surface-transpiration concept where the surface movement velocity could be chosen to equal w^1. The computational grid needs to be changed with each update of the blade profile. Thus, the aerodynamic parameters need to be transfered between old and new grid points by an accurate interpolation method. We used locally bilinear interpolation for this purpose.

Boundary conditions at the other boundaries of the computational domain (inlet, exit, parts of the airfoil surface that intentionally are prevented from changing) are the same as in the case of an analysis problem. In our case, at the inlet boundary , the stagnation pressure, stagnation temperature and the inlet flow angle are specified, while the density is computed from the interior of the domain. At the exit boundary, the static pressure is imposed, while the density and the contravariant physical components of velocity are extrapolated from the adjacent interior grid points. Along periodic boundaries, standard periodic boundary conditions are readily used since we utilized a geometrically periodic H-type grid which in turn are acceptable for sharp leading and trailing edges only.

Computed Results

Based on the method presented in this paper, a Navier-Stokes equation (NSE) inverse shape design code has been developed for linear cascades of airfoils.

The test cases No.1 and No.2 are two linear cascades for subsonic flow with different desired distributions of surface pressure coefficients (Fig. 2). Both test cases have the same inlet and exit flow conditions which are: inlet Mach number $M_{-\infty} = 0.44$, inlet angle $\alpha_{-\infty} = 30$ degrees, and exit-to-inlet pressure ratio, $p_{+\infty}/p_{-\infty} = 1.028$. The calculation was performed on a boundary-conforming H-type grid having 56 cells in the streamwise direction consisting of 13 cells between inlet and leading edge clustered towards the leading edge, 20 uniform grid cells from the leading edge to trailing edge, and 23 grid cells between the trailing edge and the exit boundary with declustering towards the exit. There were 43 grid cells in the circumferential direction. These cells were strongly clustered towards the airfoil surfaces with the high resulting maximum cell aspect ratios. The number of total time steps used was n = 40,000 since we used an explicit code. In the calculation process, when n < 20,000, the flow field was calculated by solving the direct (analysis) problem in order to create a better steady initial flow field for the inverse problem. When n = 20,000, the method solving the inverse problem is activated. Figure 3 shows the comparison of airfoil profiles generated by the NSE inverse design code for test cases No.1 and No.2. Figures 4-a, 4-b, 5-a and 5-b show the airfoil-to-airfoil velocity profiles for the two test cases at different axial locations. Figures 6-a and 6-b show the details of streamwise velocity profiles in the regions with separated flow near the suction surfaces of the two test airfoils. Figures 7-a and 7-b show the computed turbulent viscosity coefficient, μ_t, profiles at several axial locations for the two airfoils. Figures 8-a, 8-b, 9-a and 9-b show the wake velocity and the total pressure recovery coefficient, σ, profiles at several axial locations downstream of the cascade trailing edge.

Comparing the computational results of previous two cascades designed by the NSE inverse code, it can be seen that the locations of initial separation points are significantly different. The flow in test case No.1 starts separating at 60% of the chord length, while flow separation occurs at 75% of the chord length in the test case No.2. This demonstrates the capability of our inverse shape design code to create cascades of airfoils with significantly delayed flow separation.

The test case No.3 is an example for transonic flow with inlet Mach number $M_{-oo} = 0.83$, inlet angle $\alpha_{-oo} = 30$ degrees, and exit-to-inlet pressure ratio, $p_{+oo}/p_{-oo} = 1.18$. The airfoil shape of the test cascade was obtained by an inverse code which combines an inviscid flow inverse code and a modified boundary layer code[24]. In this paper, this airfoil was used as the initial shape. Surface pressure coefficients which are very close to the experimentally obtained values were adopted as the target (desired) values (Fig. 10). Figure 11 shows very good agreement between the airfoil shape used in the experiment and the shape generated using our NSE inverse design code. Figures 12 and 13 show the airfoil-to-airfoil profiles of velocity magnitudes at different axial locations. Figure 14 shows the enlarged details of the flow reversal profiles at several axial locations. It can be seen that the initial flow separation point of this cascade is at 50% of the chord length. Nevertheless, minimizing the flow separation may be quite a time consuming objective involving actual numerical optimization that is still prohibitively expensive when utilizing Navier-Stokes equation solvers. A more economical approach is to use certain fast semi-empirical rules to detect flow separation[25] in the input (target or desired) surface pressure coefficient distribution which can then be easily modified before attempting the actual inverse NSE shape design. Figure 15 shows airfoil-to-airfoil profiles of turbulent viscosity coefficient at different axial locations.. Figures 16 and 17 show the distributions of wake velocity and total pressure recovery coefficient (which can be greater[26] than 1.0) at different axial locations downstream of the cascade trailing edge. The result of this example also shows that the shock-free supercritical cascades may be designed by a full viscous inverse design code.

Conclusions

Based on a method for the flow analysis, a new method for the solution of inverse shape design was developed that is based on a complete set of Navier-Stokes equations for unsteady, compressible turbulent flows. The pressure coefficient distributions on the airfoil surfaces were taken as given boundary conditions in the inverse problem. The computations are completed directly in physical plane using the governing equations in conservative form expressed in the non-orthogonal curvilinear boundary-conforming coordinates and corresponding non-orthogonal velocity vector components. The results of these examples indicate that in this method the effect of fluid viscosity may be considered more accurately and reasonably. As a by-product of this inverse design method, the details of the flow field (flow separation regions, wake velocity profiles, etc.) are also obtained. It may be expected that in the future the present inverse shape design method will be conveniently expanded into the solution of fully three-dimensional viscous turbulent rotating flows.

Acknowledgements

The lead author gratefully acknowledges the support of K. C. Wong Education Foundation, Hong Kong, Chinese Fund of Natural Sciences, and China General Corporation of Aeronautical Industry during his six months Visiting Exchange Scientist appointment at the Department of Aerospace Engineering, The Pennsylvania State University.

References

[1]Wang, Z., Chen, H., and Zhao, X. "A Quasi-3D Design Method of Transonic Compressor Blade with the Function of Improving Velocity Distribution", 9th ISABE Congress, paper 89-7089, 1989.

[2]Zedan, M., and Sehra, A., "Application of an Inverse Design Procedure to Axial Compressor Blading", ASME paper 90-GT-67, 1990.

[3]Dulikravich, G. S., (editor), "Proceedings of the 1st International Conference on Inverse Design Concepts and Optimiz. in Engineering Sciences (ICIDES-I)", Department of Aero. Eng. and Eng. Mech., University of Texas, Austin, TX., Sept. 1984.

[4]Dulikravich, G. S., (editor), "Proceedings of the 2nd International Conference on Inverse Design Concepts and Optimiz. in Engineering Sciences (ICIDES-II)", Department of Aero. Eng., Pennsylvania State University, University Park, PA., October 1987.

[5]Dulikravich, G. S., (editor), "Proceedings of the 3rd International Conference on Inverse Design Concepts and Optimiz. in Eng. Sciences (ICIDES-III)", Washington, D.C., October 1991.

[6]Dulikravich, G. S., "Aerodynamic Shape Design and Optimization: Status and Trends," *AIAA Journal of Aircraft*, Vol. 29, No. 5, Nov./Dec., 1992, pp. 1020-1026.

[7]Slooff, J. W., (editor), "Proceedings of the AGARD Specialist's Meeting on Computational Methods for Aerodynamic Design (Inverse) and Optimization", AGARD CP-463, Loen, Norway, May 1989.

[8]Van dem Baembussche, R., (editor), "Proceedings of a Special Course on Inverse Methods for Airfoil Design for Aeronautical and Turbomachinery Applications", AGARD Report No. 780, Rhode-St.-Genese, Belgium, May 1990.

[9]Meauze, G., "An Inverse Time Marching Method for the Definition of Cascade Geometry", ASME paper 81-GT-167, 1981.

[10]Dulikravich, G. S., and Sobieczky, H., "Shockless Design and Analysis of Transonic Cascade Shapes", *AIAA Journal*, Vol. 20, No. 11, Nov. 1982, pp. 1572-1578.

[11]Hobbs, D. E., and Wingold, H. D., "Development of Controlled Diffusion Airfoils for Multistage Compressor Application", *ASME Journal of Engineering for Gas Turbines and Power*, Vol. 106, No. 2, April 1984, pp. 271-278.

[12]Dunker, R., Rechter, H., Starken, H., and Weyer, H., "Redesign and Performance Analysis of a Transonic Axial Compressor Stator and Equivalent Plane

Cascades with Subsonic Controlled Diffusion Blades", *ASME Journal of Engineering for Gas Turbines and Power*, Vol. 106, No. 2, April 1984, pp. 279-287.

[13]Luu, T. S. and Viney, B., "The Turbomachine Blading Design Achieved by Solving the Inverse Flow Field Problem", ASME paper 87-GT-215, 1987.

[14]Wang, Z., "Inverse Design Calculations for Transonic Cascades", *International Journal of Turbo and Jet Engines*, Vol. 4, No. 3-4, 1987, pp. 217-224.

[15]Wang, Z., "Solution of Transonic S_1 surface Flow by Successively Reversing the Direction of Integration of the Stream Function Equation", ASME *Journal of Engineering for Gas Turbines and Power*, Vol. 107, No. 2, April 1985, pp. 317-321.

[16]Wang, Z., "Solution of Cascade Inverse Problem Considering Viscous Influence", *Chinese Journal of Engineering Thermophysics*, Vol. 10, No. 4, 1989, pp. 390-393.

[17]Dulikravich, G. S., and Sobieczky, H., "Design of Shock-Free Compressor Cascade Including Viscous Boundary Layer Effects", ASME paper 83-GT-134, 1983.

[18]Hassan, A. A., and Dulikravich, G. S., "A Hodograph-Based Method for the Design of Shock-Free Cascades", *International Journal for Numerical Methods in Fluids*, Vol. 7, No. 3, March 1987, pp. 197-213.

[19]Wu, C.-H., "Basic Equations of Three-Dimensional Flow in Turbomachines Expressed with Respect to Nonorthogonal Curvilinear Coordinates and Nonorthogonal Velocity Components and its Methods of Solution", 3rd ISABE Congress, 1976.

[20]Wang, Z., and Zhang, W., "Numerical Analysis of Cascade Viscous Flow Using Navier-Stokes Equations Expressed by Nonorthogonal Curvilinear Coordinates", CSET paper 932032; to appear in *Chinese Journal of Engineering Thermophysics*, 1994.

[21]Chen, H., "Conservative Form of Momentum Equations Using Nonorthogonal Curvilinear Coordinates", Proceedings of Commemorating Symposium in honor of Prof. Wu Chung-Hua, 1993.

[22]Baldwin, B. S., and Lomax, H., "Thin Layer Approximation and Algebraic Model for Separated Turbulent Flows", AIAA paper 78-257, 1978.

[23]MacCormack, R. W., "The Effect of Viscosity in Hypervelocity Impact Cratering", AIAA paper 69-354, 1969.

[24]Wang, Z., Chung, Y., Wu, G., and Zhang, W., "Design and Testing of Shock-Free Supercritical Cascade", *Chinese Journal of Engineering Thermophysics*, Vol. 13, No. 4, 1992, pp. 375-379.

[25]Dulikravich, G. S., "A Criteria for Surface Velocity Specification in Aerodynamic Shape Design", AIAA paper 90-0124, Reno, NV, January 1990.

[26]Mer, D. J., Baines, N. C., Oldfield, M. L. G., and Dickens, T. E., "An Examination of the Contributions to Loss on a Transonic Turbine Blade in Cascade", ASME J. of Turbomachinery, Jan. 1992, Vol. 114.

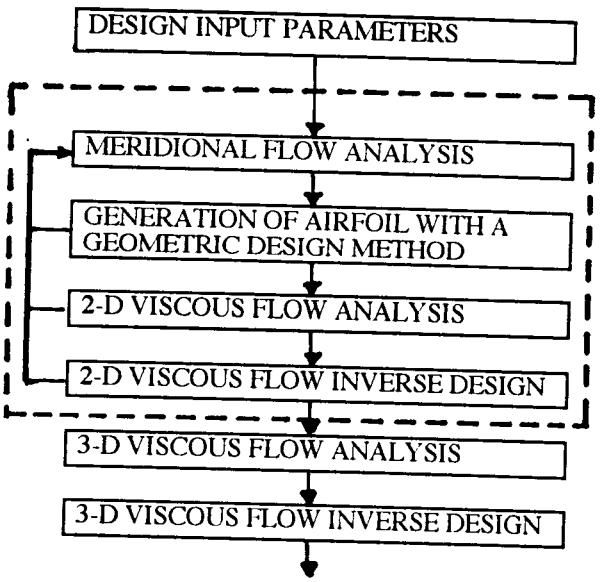

FIGURE 1. TURBOMACHINERY BLADE AERODYNAMIC SHAPE DESIGN PROCESS: (_ _ _) QUASI 3-D DESIGN SYSTEM

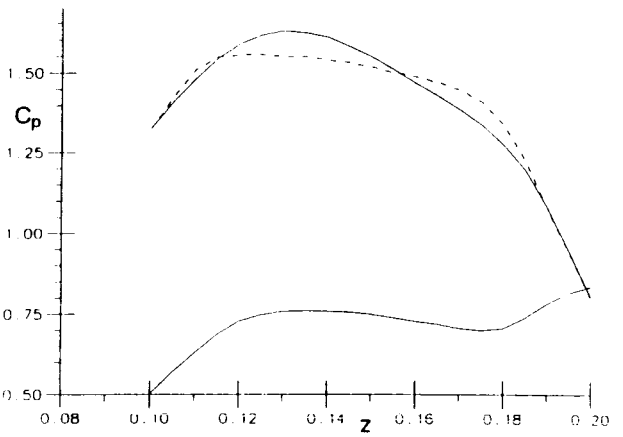

FIGURE 2. TARGET SURFACE PRESSURE COEFFICIENT DISTRIBUTIONS: (_____) TEST CASE NO.1; (_ _ _) TEST CASE NO.2.

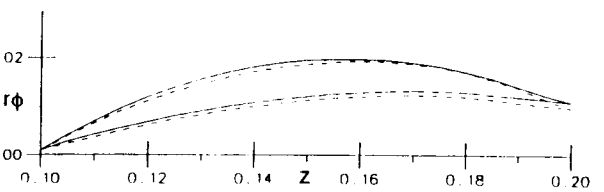

FIGURE 3. LINEAR CASCADE AIRFOIL SHAPES GENERATED BY N-S-E INVERSE DESIGN CODE: (_____) TEST CASE NO.1; (_ _ _) TEST CASE NO.2.

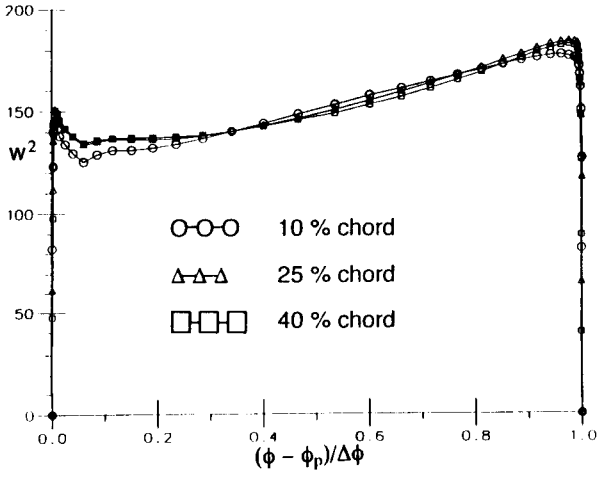

a

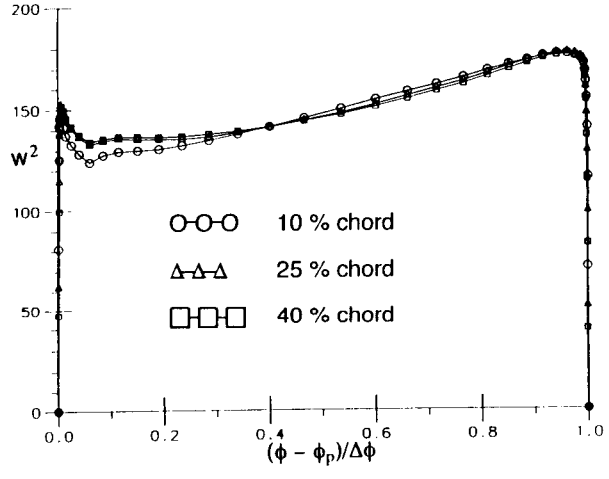

b

FIGURE 4. STREAMWISE VELOCITY PROFILES AT DIFFERENT AXIAL LOCATIONS:
a) TEST CASE NO.1; b) TEST CASE NO.2.

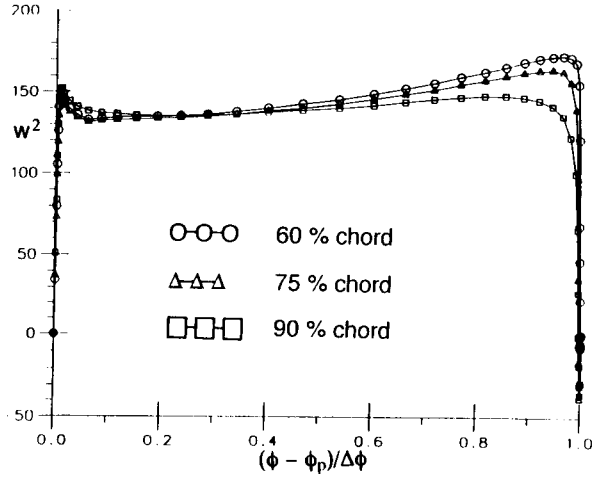

a

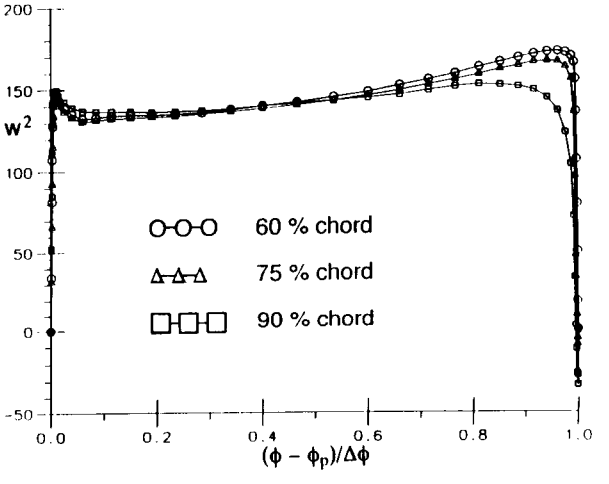

b

FIGURE 5. STREAMWISE VELOCITY PROFILES AT DIFFERENT AXIAL LOCATIONS:
a) TEST CASE NO.1; b) TEST CASE NO.2.

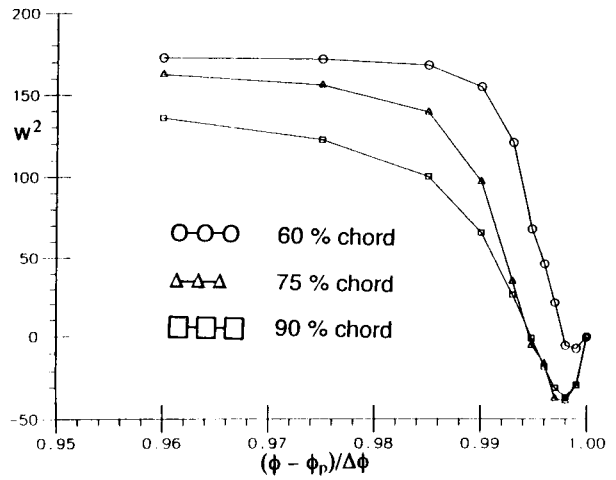

a

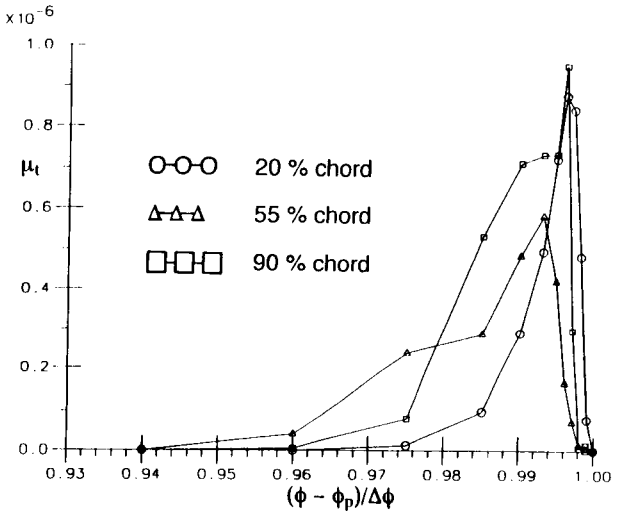

a

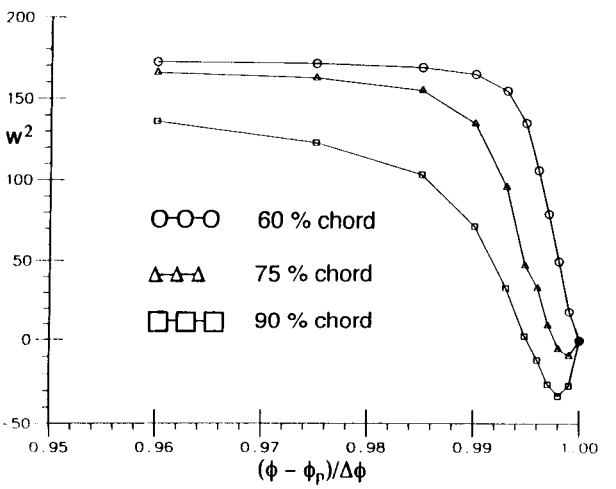

b

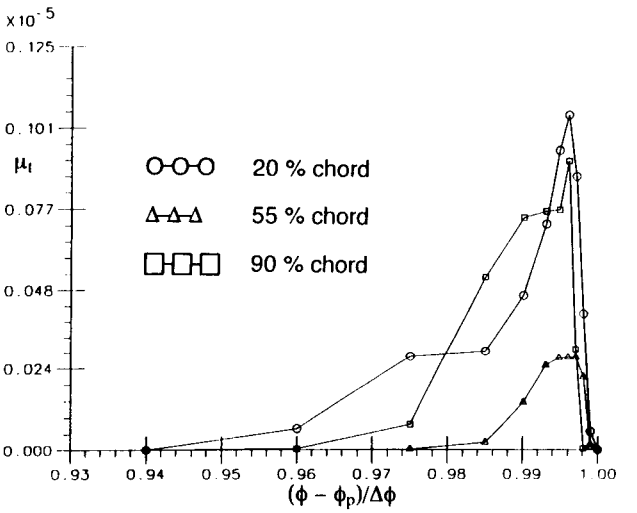

b

FIGURE 6. DETAIL OF STREAMWISE VELOCITY PROFILES AT DIFFERENT AXIAL LOCATIONS: a) TEST CASE NO.1; b) TEST CASE NO.2.

FIGURE 7. PROFILES OF TURBULENT VISCOSITY COEFFICIENTS AT DIFFERENT AXIAL LOCATIONS: a) TEST CASE NO.1; b) TEST CASE NO.2.

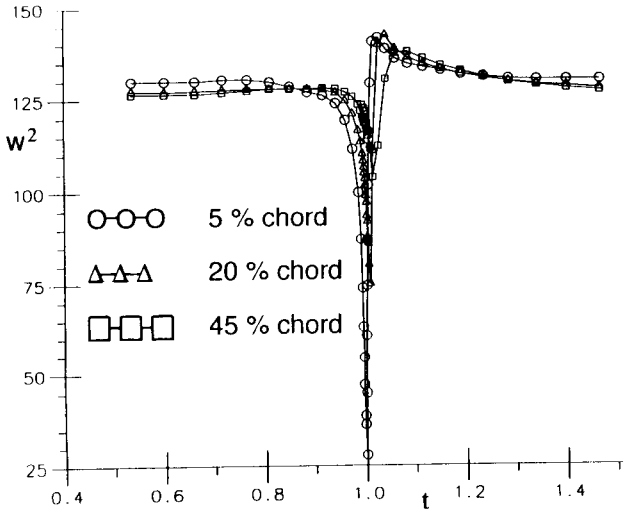

a

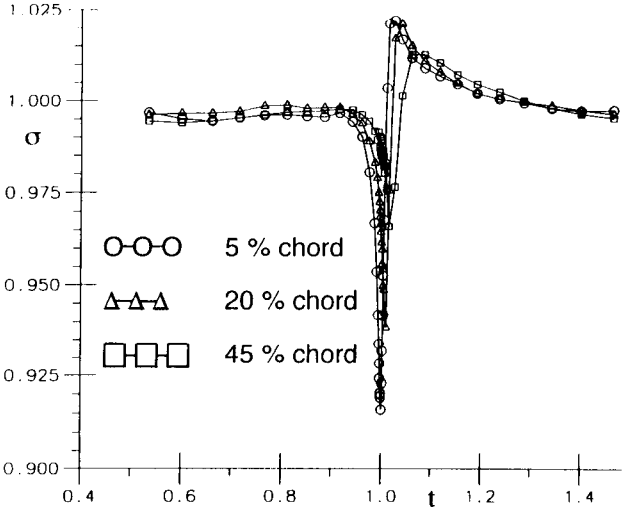

a

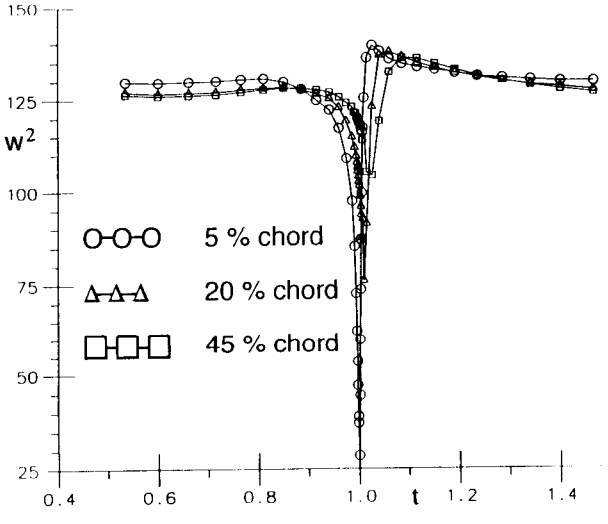

b

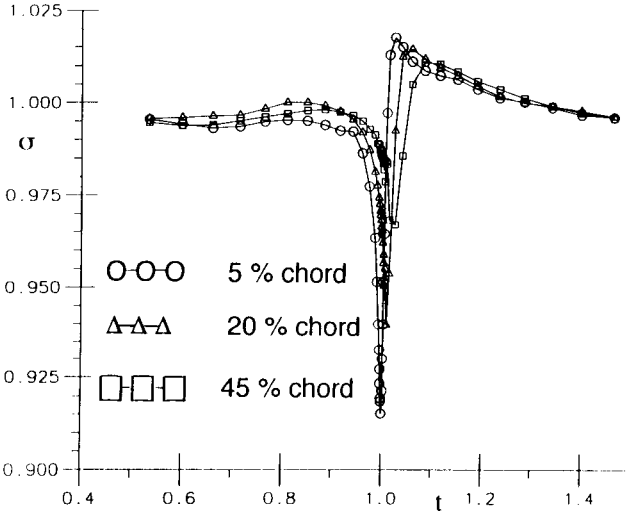

b

FIGURE 8. WAKE STREAMWISE VELOCITY PROFILES AT DIFFERENT AXIAL LOCATIONS DOWNSTREAM OF THE TRAILING EDGE: a) TEST CASE NO.1; b) TEST CASE NO.2.

FIGURE 9. WAKE TOTAL PRESSURE RECOVERY PROFILES AT DIFFERENT AXIAL LOCATIONS DOWNSTREAM OF THE TRAILING EDGE: a) TEST CASE NO.1; b) TEST CASE NO.2.

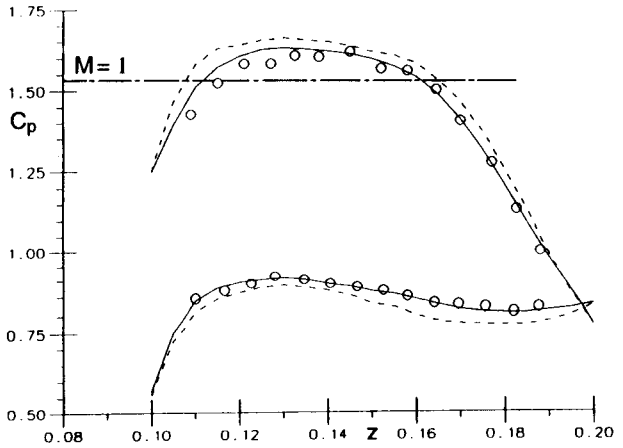

FIGURE 10. SURFACE PRESSURE COEFFICIENT DISTRIBUTIONS FOT TEST CASE NO.3: (O O O) EXPERIMENT; (_) TARGET FOR OUR N-S-E INVERSE DESIGN; (_ _ _) TARGET FOR THE VISCOUS/INVISCID INVERSE DESIGN CODE (WANG ET AL., 1992).

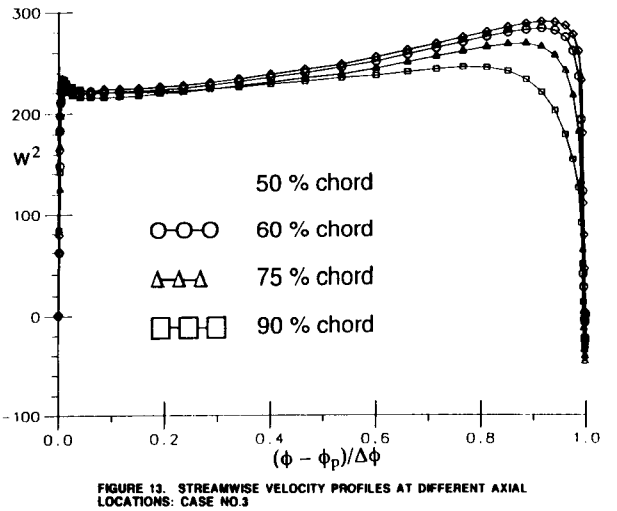

FIGURE 13. STREAMWISE VELOCITY PROFILES AT DIFFERENT AXIAL LOCATIONS: CASE NO.3

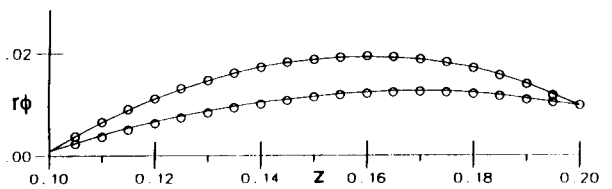

FIGURE 11. COMPARISON OF AIRFOIL SHAPE USED IN THE EXPERIMENT (_____) AND THE SHAPE GENERATED BY OUR INVERSE DESIGN N-S-E CODE (O O O).

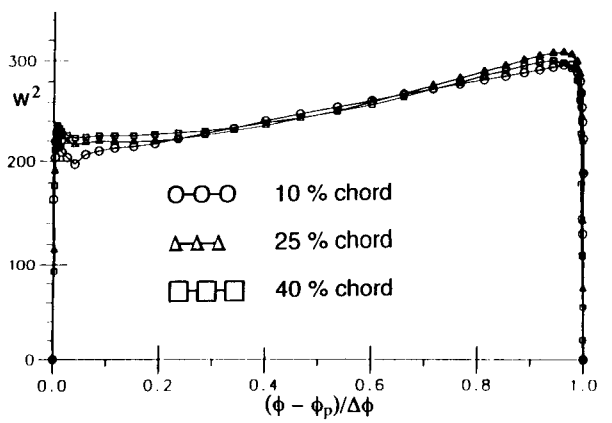

FIGURE 12. STREAMWISE VELOCITY PROFILES AT DIFFERENT AXIAL LOCATIONS: CASE NO.3

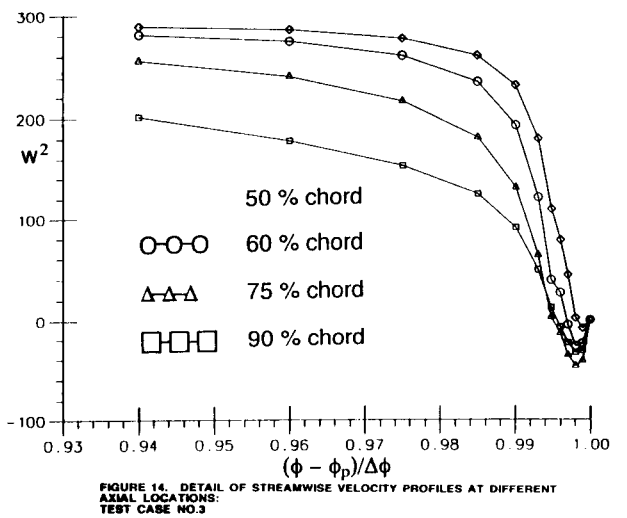

FIGURE 14. DETAIL OF STREAMWISE VELOCITY PROFILES AT DIFFERENT AXIAL LOCATIONS: TEST CASE NO.3

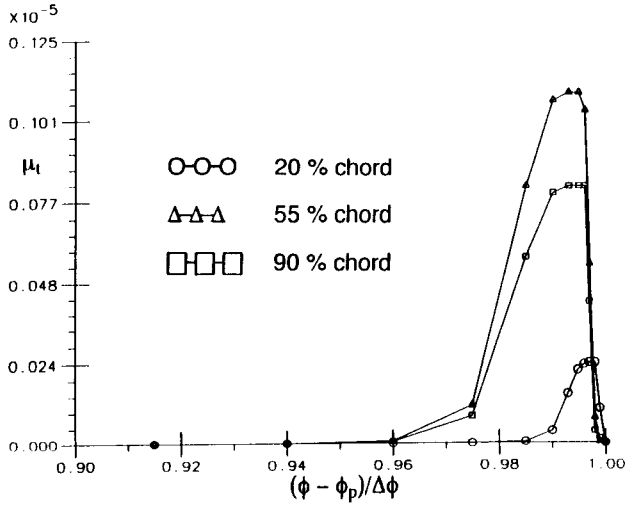

FIGURE 15. PROFILES OF TURBULENT VISCOSITY COEFFICIENTS AT DIFFERENT AXIAL LOCATIONS: TEST CASE NO.3

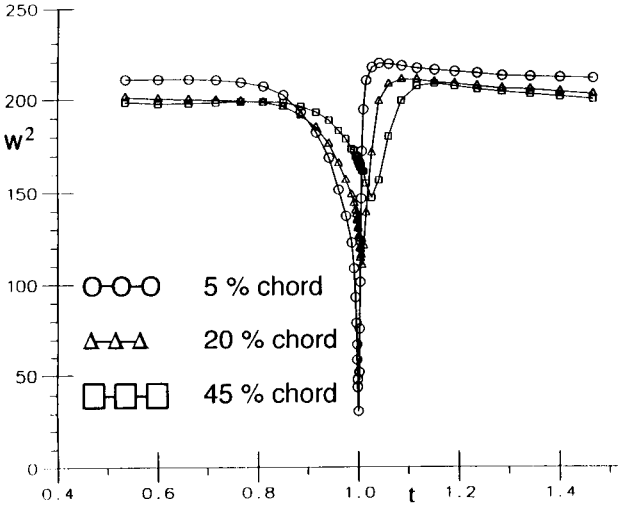

FIGURE 16. WAKE STREAMWISE VELOCITY PROFILES AT DIFFERENT AXIAL LOCATIONS DOWNSTREAM OF THE TRAILING EDGE: TEST CASE NO.3

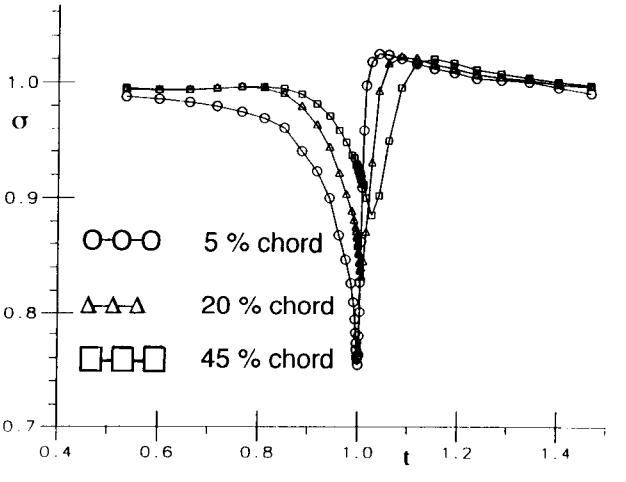

FIGURE 17. WAKE TOTAL PRESSURE RECOVERY PROFILES AT DIFFERENT AXIAL LOCATIONS DOWNSTREAM OF THE TRAILING EDGE: TEST CASE NO.3